Hybrid lipid/polymer nanoparticles for pulmonary delivery of siRNA: development and fate upon *in vitro* deposition on the human epithelial airway barrier

I. d'Angelo[a], G. Costabile[b, c], E. Durantie[c], P. Brocca[d], V. Rondelli[d], A. Miro[b], F. Quaglia[b], A. Petri-Fink[c], B. Rothen-Rutishauser[c] and F. Ungaro[b]

The down-regulation of genes directly involved in the pathogenesis of severe lung diseases through siRNA delivery to the lung has gained recently tremendous research interest. Nevertheless, adequately engineered inhalable siRNA formulations are required to translate this approach *in vivo*. Here, we propose novel hybrid lipid/polymer hybrid nanoparticles (hNPs) for pulmonary siRNA delivery consisting of a poly(lactic-co-glycolic) acid (PLGA) core surrounded by a dipalmitoyl phosphatidylcholine (DPPC) shell. A preliminary formulation study allowed to select optimized "muco-inert" PLGA/DPPC hNPs, comprising or not poly(ethylenimine) (PEI) as third component, which displayed mean hydrodynamic diameters of 150 nm, with a low polydispersity index (~0.1) and a negative zeta potential (~-25 mV). A combination of siRNA of interest for cystic fibrosis (CF), against α and β subunits of the sodium transepithelial channe,ł was entrapped with high efficiency in optimised hNPs containing or not PEI. siRNA-loaded hNPs displayed a peculiar triphasic release lasting for 5 days, which slowed down in the presence of PEI. Both formulations showed optimal *in vitro* aerosol performance after delivery with a vibrating mesh nebulizer and *in vitro* long-term stability upon incubation with artificial CF mucus. The fate and the effects of hNPs upon aerosolization on a triple cell co-culture model (TCCC) mimicking human epithelial airway barrier were assessed. Cell uptake studies confirmed the ability of fluorescently labelled hNPs to be internalized inside cells of the epithelial airway barrier. As measured by lactate dehydrogenase (LDH) release 24 h after treatment, PLGA/DPPC hNPs did not exert any cytotoxic effect towards TCCC. Furthermore, TCCC exposure to PLGA/DPPC hNPs did not result in a significant increase of tumor necrosis factor (TNF)-alpha release after 24 h, suggesting no acute pro-inflammatory effect. Overall, results demonstrate the great potential of PLGA/DPPC hNPs as carriers for siRNA delivery on the human epithelial airway barrier, prompting towards investigation of their therapeutic effectiveness in CF.

Introduction

RNA interference refers to the inhibition of gene expression by small, double-stranded RNA molecules (small interference RNA or siRNA) that direct the mRNA machinery to degrade a specific mRNA. siRNA therapeutics have many advantages in terms of clinical applications, the first of which is their virtual potential to specifically silence any gene underlying more or less complex pathologies.[1,2] In particular, severe lung diseases, such as lung cancer and cystic fibrosis (CF), nowadays represent a very important area of application for siRNA-based therapies.[3] Nevertheless, to harness the full potential of the siRNA strategy for severe lung diseases, an appropriately designed delivery system is mandatory.[4,5] Naked siRNAs have a half-life of less than an hour in human plasma and are often unable to penetrate cellular membranes. In fact, cellular uptake and the escape from endo-lysosomes are critical steps before siRNA reaches the cytoplasm, where its target is located. Conceiving siRNA for local delivery by inhalation, the presence of high mucin, DNA and actin concentrations, making airway mucus a very complex barrier, should also be taken into account.[4,5] Thus, optimal inhalable formulations are required to: i) enhance siRNA stability; ii) overcome lung cellular and non-cellular barriers; iii) increase siRNA availability at the target level. Amid advanced drug delivery systems, the encapsulation of siRNA into colloidal carriers is considered as a very promising formulation approach for inhaled treatment of severe lung diseases.[4,5]

The most studied nanocarriers for the delivery of siRNA are based on lipids and comprise either the entrapment of siRNA into liposomal vescicles or, more often, its complexation with positively charged lipids (i.e., lipoplexes).[4,6] Thanks to their ability to enhance cell uptake and their good tolerance in the pulmonary tract, these carriers gained tremendous interest for pulmonary delivery, both in the scientific and industrial environment.[7] Nevertheless, the application of lipid-based carriers is strongly limited by the low loading efficiencies, especially for hydrophilic drugs and, depending on their composition, by poor stability and drug release control *in vitro/in vivo*.[7,8]

Biodegradable polymeric nanoparticles (NPs) represent a viable alternative for pulmonary delivery of nucleic acid therapeutics,[9] since they may overcome most of the lipid carrier limitations. Among the polymers of interest for lung delivery of siRNA, poly(lactic-co-glycolic) acid (PLGA) seems very promising.[5,9] In fact, PLGA-based NPs may provide protection of the therapeutic cargo from enzymatic degradation, prolonged release (i.e., decreased number of administrations) and improved retention in the lungs.[10,11]

In the attempt to combine the most valuable properties of both lipid and polymeric nanocarriers, hybrid lipid–polymer nanoparticles (hNPs) are gaining considerable interest.[12,13] Along these lines, our aim was to design and to optimize hNPs consisting of a PLGA core surrounded by a dipalmitoylphosphatidylcholine (DPPC) shell. hNPs have been further engineered with poly(ethylenimine) (PEI), introduced as a third component to assist siRNA entrapment in the hNPs and to increase cell uptake.[14] A preliminary formulation study allowed to select optimized "muco-inert" PLGA/DPPC hNPs containing or not PEI displaying optimal *in vitro* aerosol performance. A particular attention was devoted to the ability of the carrier to penetrate inside the airway mucus barrier through a combination of analytical techniques, that is turbidimetry assessment, dynamic light scattering (DLS) and small-angle X-ray scattering (SAXS). To allow a proof of principle of their potential for siRNA delivery to the lung, selected formulations were loaded with therapeutic siRNA of interest for CF therapy, that is a combination of siRNA against α and β subunits of the sodium transepithelial channel (ENaC).[15,16] siRNA-loaded hNPs were fully characterized for size, zeta potential, entrapment efficiency and *in*

vitro release kinetics. Finally, a thorough *in vitro* study allowed to assess the fate and the effect of hNPs upon aerosolization on a triple cell co-culture model (TCCC) grown at air-liquid interface (ALI) mimicking the human airway epithelial barrier.[17]

Experimental Methods

Materials

Resomer® RG 502H (uncapped PLGA 50:50, inherent viscosity 0.16 0.24 dl/g) was purchased from Evonik Industries AG (Germany). Rhodamine-labeled PLGA was synthesized as previously described.[18] 1,2-dipalmitoyl-sn-glycero-3- phosphocholine (DPPC) was a kind gift of Lipoid GmbH (Switzerland). siRNA (siGENOME Human SCNN1A and SCNN1B) was purchased from Dharmacon (GE Healthcare). Ph.Eur. grade mannitol (Pearlitol® C160) was kindly gifted by Roquette Italia S.p.a. (Italy). Egg yolk emulsion, deoxyribonucleic acid sodium salt from calf thymus (DNA), diethylenetriaminepentaacetic acid (DTPA), phosphate buffer salts, branched polyethylenimine (PEI; 25 KDa), potassium chloride, rhodamine B (Rhod-B), RPMI 1640 amino acid solution, sodium chloride, mucin from porcin stomach were purchased from Sigma Aldrich (USA). Methylene chloride and ethanol 96 % (v/v) were supplied by Carlo Erba (Italy).

Production of PLGA/DPPC hybrid nanoparticles

PLGA/DPPC hNPs were prepared by emulsion/solvent diffusion technique. Briefly, a water in oil emulsion (w/o) was achieved adding 100 μl of water to 1 mL of methylene chloride containing PLGA (1% w/v) and DPPC at different DPPC/PLGA ratios (1:10; 1/20; 1:50; 1:100; 1:150), under vortex mixing (2400 min^{-1}, Heidolph, Germany). When needed, PEI was added to the internal water phase at the theoretical loading of 0.016 % (0.016 mg *per* 100 mg of hNPs). Just after mixing, the w/o emulsion was added to 12.5 mL of ethanol 96 % (v/v) under moderate magnetic stirring, leading to immediate nanoparticle precipitation (Table 1). Then, the formulation was diluted with 12.5 mL of Milli-Q water under stirring for 10 min. Afterwards, residue organic solvent was removed by rotary evaporation under vacuum at 30ºC (Heidolph VV 2000, Germany). hNPs were isolated from the resulting hNP colloidal dispersion (5 mL) by centrifugation at 7000 rcf for 20 minutes at 4°C (Hettich Zentrifugen, Germany) and dispersed in Milli-Q water.
siRNA-loaded hNPs were prepared in optimized formulation conditions at a theoretical loading of 1 nmol/100 mg of PLGA (N/P theoretical ratio of 10 in PEI-modified hNPs) by adding siRNA to the internal water phase.
Fluorescently-labelled hNPs ($DPPC_{Rhod}$ and $PEI/DPPC_{Rhod}$) were prepared using rhodamine-labelled PLGA (PLGA-Rhod) in the organic phase at 10% w/w with respect to the total PLGA amount.

Characterization of PLGA/DPPC hybrid nanoparticles

Size and zeta potential. The hydrodynamic diameter (D_H), the polydispersity index (PI) and the zeta potential (ζ potential) of hNPs were determined by dynamic light scattering (DLS), with a Malvern Zetasizer Nano ZS (Malvern Instruments, UK). Results are expressed as mean value ± SD of triplicate measurements on different batches.

siRNA loading inside hNPs. siRNA actual loading was measured indirectly by quantitation of non-encapsulated siRNA. Briefly, just after production hNPs were collected by centrifugation (7000 rcf for 20 minutes at 4°C) and the supernatant was analysed for siRNA content using Quant-IT™ RiboGreen® reagent (Thermo Fisher Scientific) according to the manufacturer's instructions. Quantitative analysis was performed by spectrofluorimetry at λ_{ex} 480 nm/λ_{em} 520 nm (EnVision® Multilabel Plate Readers, PerkinElmer Inc., USA). Results are reported as actual loading (nmol of encapsulated siRNA *per* mg of hNPs) and encapsulation efficiency (actual loading/theoretical loading x 100) ± standard deviation (SD) of values collected from three different batches.

SAXS spectroscopy. Synchrotron Small Angle X-ray scattering (SAXS) measurements were performed at the ID02 high-brilliance beamline [19] at the ESRF (Grenoble, France), with a beam cross section of 200μm x 400 μm and wavelength λ = 0.1 nm, using two different sample detection distances: 1 and 6m. The range of investigated momentum transfer, $q = (4\pi/\lambda)\sin(\theta)$, was $0.0116\ nm^{-1} < q < 6.43\ nm^{-1}$, where 2 θ is the scattering angle. All measurements were performed at T = 25 °C. Samples were put in plastic capillaries (KI-BEAM, ENKI srl) with 2 mm internal diameter, 0.05 mm wall thickness, closed with polyethylene caps. Capillaries were then mounted horizontally onto the sample holder. Sample concentration was 10 mg/ml. The exposure time of each measurement was 0.1 s, and spectra were checked for radiation damage. The measured SAXS profiles report the scattered radiation intensity as a function of the momentum transfer, q, where 1 m and 6 m sample-to-detector distance spectra were merged. Solvent subtraction was obtained by measuring water filled capillaries and empty capillaries.

***In vitro* interaction with mucin.** Turbidimetric measurement of mucin/nanoparticle interactions was performed as previously described.[20,21] Briefly, a saturated solution of type II mucin was prepared by centrifugation at 6000 rcf for 20 min of a mucin dispersion in water (0.08 % w/v) stirred overnight. Then, hNPs were dispersed in the mucin solution at a concentration of 1 mg/mL by vortexing for 1 min. The turbidity of the mucin/hNPs mixtures was measured by spectrophotometric analysis at 650 nm at time 0 and after incubation for 30 and 60 minutes at room temperature. Reference absorbance (ABS) of mucin and 1 mg/mL hNP dispersions in water were also evaluated. Experiments were run in triplicate and results are expressed as ABS at 650 nm ± SD over time.
The interactions of hNPS with mucin were further investigated by DLS as previously reported.[22] Briefly, hNPs were dispersed in the mucin stock solution (0.08% w/v) at a concentration of 1 mg/mL and the dispersions examined with the Malvern Zetasizer Nano ZS (Malvern Instruments, UK). Experiments were run in triplicate and results are reported as representative size distribution by intensity of hNPs in mucin *versus* hNPs in water. The size distribution profile of the mucin solution was also recorded as control.

Particle-stability in artificial mucus. To assess the stability of siRNA-loaded hNPs and their ability to diffuse inside airway mucus without dissolution, SAXS analyses were performed also on hNP dispersions in the presence of artificial mucus (AM). AM was prepared as previously reported[21] by adding 25 μL of sterile egg yolk emulsion, 25 mg of mucin, 20 mg of DNA, 30 μL of aqueous DTPA (1 mg/mL), 25 mg NaCl, 11 mg KCl and 100 μL of RPMI 1640 to 5 mL of water. The dispersion was stirred until a homogenous mixture was obtained. For stability studies, aqueous dispersions of siRNA-loaded hNPs (10 mg/mL) were mixed with AM in a 1:3 volume ratio for a total 40 μL sample volume. After 1 h equilibration time, SAXS was performed as described above. Particle structure after 12 h interaction with artificial mucus was verified by repeated SAXS measurements.

***In vitro* release kinetics of siRNA.** siRNA-loaded hNPs were characterized for *in vitro* siRNA release kinetics in phosphate buffer (120 mM NaCl, 2.7 mM KCl, 10 mM Na_2HPO_4) at pH 7.2 (PBS). Release studies were performed upon dilution of hNP dispersions in

PBS to a theoretical siRNA concentration of 0.2 nmol/mL. hNP dispersions were incubated in a horizontal-shaking water bath at 40 rpm and 37°C (ShakeTemp SW 22, Julabo, Italy). At scheduled time intervals, samples were centrifuged at 7000 rcf for 20 min at 4°C to isolate hNPs, the release medium was withdrawn and analysed for siRNA content by spectrofluorimetric analysis as described for actual loading. The medium was replaced by the same amount of fresh PBS. Experiments were carried out in triplicate and results expressed as percentage of siRNA released from hNPs ± SD.

***In Vitro* Aerosol Performance.** The aerosolization properties of fluorescently-labelled $DPPC_{Rhod}$ and $PEI/DPPC_{Rhod}$ hNP dispersions were investigated *in vitro* after delivery from the Aeroneb® Go nebuliser (Aerogen Ltd., Ireland) by a Next Generation Impactor (NGI) (Copley Scientific, UK) according to the *Comité Européen de Normalization* (CEN) standard methodology for nebulizer systems with sampling at 15 L/min and insertion of a filter in micro-orifice collector (MOC).[23] Briefly, 1 mL of hNP dispersion was transferred to the reservoir of the nebulizer, which was connected to the induction port of the NGI. The nebulizer was operated at 15 L/min, and the aerosol was drawn through the impactor for 5 minutes, until dryness.

The amount of fluorescent hNPs remaining inside the nebulizer chamber, deposited on the seven NGI collection cups and in the induction port was quantitatively recovered in NaOH 0.5 M. After stirring at room temperature for 1 h, the amount of fluorescent hNPs in the resulting solutions was determined by spectrofluorimetric analysis at λ_{ex}=553 nm and λ_{em}=577 nm (GloMax® Explorer, Promega, Italy) as previously reported.[21] Calibration curves were derived by analysing serial dilutions of $DPPC_{Rhod}$ or $PEI/DPPC_{Rhod}$ standard solutions prepared from a stock of hNPs degraded in NaOH 0.5 M. The linearity of the response was verified over the concentration range 2–200 µg/mL ($r^2 \geq 0.999$). Each experiment was run in triplicate.

The emitted dose (ED) was measured as the difference between the total amount of hNPs initially placed and the amount remaining in the nebulizer chamber. Upon emission, the experimental mass median aerodynamic diameter ($MMAD_{exp}$) and the geometric standard deviation (GSD) were calculated according to the European Pharmacopoeia deriving a plot of cumulative mass of particle retained in each collection cup (expressed as percent of total mass recovered in the impactor) *versus* the cut-off diameter of the respective stage.

The fine particle fraction (FPF) was calculated taking into account the amount of hNPs deposited on stages 3 -7 ($MMAD_{exp}$ < 5.39 µm) compared to the initial amount loaded into the nebulizer chamber, while the respirable fraction (RF) referred to the total amount recovered from the NGI.

***In vitro* studies on airway triple cell co-cultures**

All *in vitro* exposure experiments were conducted with a three dimensional triple cell co-culture model mimicking the human epithelial airway barrier comprising human bronchial epithelial cells (16HBE14o-), human blood monocyte-derived macrophages (MDM) and dendritic cells (MDDC).[17]

16HBE14o- cell cultures. 16HBE14o- cells were kindly provided by Dieter Gruenert (passage number P2.54; University California, San Francisco, CA, USA). Cells were maintained in minimum essential media (MEM) 1X medium (with Earle's Salts, 25 mM HEPES and without L-glutamine; Gibco BRL), supplemented with 1 % L-glutamine, 1 % penicillin/streptomycin and 10 % foetal calf serum. For experimental cultures, cells were seeded at a density of 0.5 x 10^6 cells/insert on transparent BD Falcon cell culture inserts (surface area of 0.9 cm^2, pores with 3.0 µm diameter, PET membranes for 12-well plates). The cell culture inserts were pre-treated with 150 µL of a fibronectin coating solution containing 0.1 mg/mL bovine serum albumin (Sigma-Aldrich), 1 % Type I bovine collagen (BD Biosciences) and 1 % human fibronectin (BD Biosciences) in LHC Basal Medium (Sigma-Aldrich). Inserts were placed in BD Falcon tissue culture plates (12-well plates) with 0.5 mL medium in the upper and 1 mL in the lower chamber. The cells were kept at 37 °C in 5 % CO_2 humidified atmosphere for 7 days (medium changed after 3–4 days).

Triple cells co-culture (TCCC) system. To produce the TCCC *in vitro* model, 16HBE14o- cells cultures were supplemented on the apical side with MDM and on the baso-lateral side with MDDC derived from human blood as previously reported.[17,24] Briefly, 16HBE14o- were cultured as described above. At 7 days, the medium was removed from the upper and lower chamber, the inserts turned up-side down and the bottom was abraded carefully with a cell scraper. The inserts were then incubated with 65 µL medium containing 83 x 10^4 MDDC/mL on the basal side for two hours. Afterwards, the inserts turned around again and placed in BD Falcon™ tissue culture plates (12-well plates). In the lower chamber 1.5 mL of medium and at the apical side of the TCCC 500 µL medium containing 2.5 x 10^4 MDM/mL was added. Once again the systems were incubated for two hours to allow the macrophages to attach. The complete TCCC systems were kept with 1.5 mL of medium in the lower chamber and 0.5 mL in the upper chamber at 37 °C in 5 % CO_2 humidified atmosphere for 24 h.

To establish the air-liquid interface (ALI), the medium in the upper chamber of the TCCC systems was removed 24 h prior to exposure in the Vitrocell® Cloud, while the medium in the lower chamber was replaced by 0.6 mL of fresh medium.

***In vitro* TCCC exposure to aerosolized nanoparticles.** Cell exposure to hNPs at ALI was carried out with the Vitrocell® Cloud system (Vitrocell Systems GmbH, Germany). Briefly, the Vitrocell® Cloud consists of three main components: a nebulizer, an exposure chamber and a flow system with an incubation chamber providing suitable temperature and humidity cell culture conditions. The aerosol is generated into the exposure chamber by a perforated vibrating membrane nebuliser (Aeroneb®Pro, with a span of 2.5-6.0 µm volume mean diameter). Before each experiment, freeze-dried hNPs were dispersed in 0.5 µM sodium chloride. For TCCC exposure to low hNP concentrations, 200 µL of a 0.5 mg/mL hNP dispersions were aerosolized (~0.1 mg of hNPs). For high hNP concentrations, TCCC were exposed to further 400 µL (2 x 200 µL) of a 0.9 mg/mL hNP dispersion (~0.5 mg of hNPs). TCCC exposed to 0.5 µM sodium chloride and mannitol aqueous solutions were used as controls. Following the exposure in the chamber (10 and 30 min for 0.1 and 0.5 mg of hNPs, respectively), the inserts were immediately placed in new BD Falcon 12- well tissue culture plates containing 0.6 mL of fresh medium for cell uptake studies, cytotoxicity assay and tumor necrosis factor alpha (TNF-α) release.

Nanoparticle deposition efficiency. The amount of hNPs deposited upon nebulization inside the Vitrocell® Cloud was assessed. To this purpose, glass coverslips (24 x 24 mm) were placed onto the compartments for cell culture inserts and exposed to different amounts of aerosolized rhodamine-labelled $DPPC_{Rhod}$ and $PEI/DPPC_{Rhod}$ hNPs. After the exposure, coverslips were removed

and rinsed with NaOH 0.5 M (500 µL). After stirring at room temperature for 1 h, the amount of fluorescent hNPs in the solutions was quantified by spectrofluorimetric analysis as described for *in vitro* aerosol performance. Results are reported as µg of hNP_S deposited *per* cm^2 ± SD of values collected from three separate experiments.

Stability of hNPs upon aerosolization. Transmission electron microscopy (TEM) analysis was performed on hNP samples before and after nebulization. To this purpose, TEM copper grid (Plano, Germany) were exposed in the Vitrocell® Cloud system to different amounts of aerosolized empty DPPC, empty PEI/DPPC, siRNA/DPPC and siRNA-PEI/DPPC hNPs. After air drying, representative images of both the stock hNP dispersions before nebulization and the deposited samples were captured using a Tecnai F20 transmission electron microscope (FEI, Eindhoven, The Netherlands) equipped with an Ultra- Scan 1000XP 2 k CCD camera (Gatan Inc., Pleasanton, USA).

Cell uptake studies. The TCCC was exposed to different amounts of aerosolized rhodamine-labelled $DPPC_{Rhod}$ and $PEI/DPPC_{Rhod,}$ hNPs. After 24 h post-exposure, TCCC were fixed for 15 min with 3 % paraformaldehyde in phosphate buffered saline (PBS) at room temperature and cells were washed three times in PBS. The F-actin cytoskeleton and the DNA of all cells were stained with phalloidin (ALEXA 488) (Molecular Probes, Life Technologies Europe B.V., Switzerland) and 4',6- diamidin-2-phenylindol (DAPI) (1 µg/mL) in a 1:100 and 1:50 dilution in 0.3% Triton X-100 in PBS, respectively. For microscopy, membranes were embedded in Glycergel (DAKO Schweiz AG, Baar, Switzerland). Sample analysis was performed with an inverted Zeiss confocal laser scanning microscope 710 (LSM, Axio Observer.Z1). Representative images (z-stacks) were recorded at 3 independent fields of view for each sample. Image processing was achieved using the 3D reconstruction software IMARIS LAS AF Lite version (Leica software). **TEM?**

Cytotoxicity assay. The TCCC was exposed to different amounts of aerosolized siRNA/DPPC and siRNA-PEI/DPPC and corresponding empty hNPs. After 24 h post-exposure at 37 °C, lactate dehydrogenase (LDH) release by the TCCC, indicative of cell membrane damage, was assessed by the LDH cytotoxicity detection kit (Roche Applied Science, Germany) according to the manufacturer's guidelines. The test was performed in triplicates and evaluated in comparison to the negative controls, which are TCCC exposed to aqueous solutions of 0.5 µM sodium chloride or mannitol at the same concentrations of hNP dispersions. As a positive control, TCCC were treated with 100 µL of 0.2 % Triton X-100 in PBS on the apical side and incubated for 24 h at 37 °C, 5 % CO_2.

Tumor necrosis factor-α release. The potential pro-inflammatory response was also investigated after 24 h post-exposure to hNPs by quantifying the release of TNF-α using an ELISA kit (R&D Systems) according to the manufacturer's protocol. As a positive control, TCCC were treated with 600 µL of 1 µg/mL lipopolysaccharide (LPS) in PBS on the apical side and incubated for 24 h at 37 °C, 5 % CO_2.

Data analysis. Results of cell studies are expressed as mean value ± standard error mean (S.E.M.) (n=3). The significance of differences was determined with the software Kaleidagraph using One-Way Analysis of Variance (ANOVA) followed by Bonferroni post-hoc test. A p value < 0.05 was considered significant.

Results

Development studies of PLGA/DPPC hNPs for siRNA loading

In depth formulation studies were performed on empty hNPs to establish the optimal ratio between the selected components, i.e. PLGA, DPPC and PEI. Overall hNP properties are reported in Table 1.

A

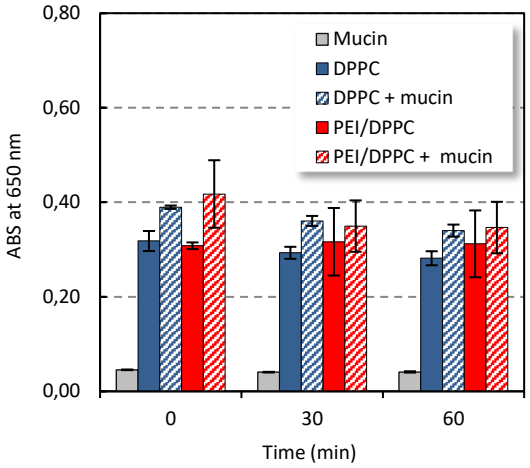

B

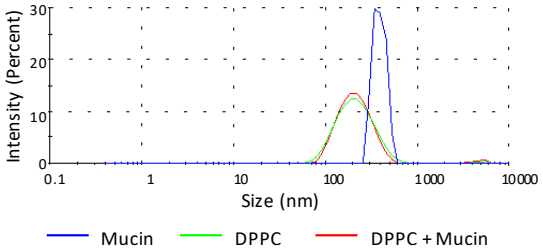

C

Table 1. Composition, size, polydispersity index and zeta potential of empty PLGA/DPPC and PEI/PLGA/DPPC hNPs.

Formulation	PEI theoretical loading (mg/100 mg of hNP)	DPPC/PLGA ratio (w/w)	Hydrodynamic diameter (D_H) (nm ± SD)	Polydispersity index (PI) (mean ± SD)	Zeta Potential (mV ± SD)
DPPC10	-	1/10	151.3 ± 21.3	0.127 ± 0.079	-25.3 ± 0.5
DPPC20	-	1/20	149.7 ± 2.1	0.083 ± 0.006	-23.2 ± 2.4
DPPC50	-	1/50	135.4 ± 17.2	0.088 ± 0.008	-24.3 ± 6.0
DPPC100	-	1/100	158.9 ± 7.1	0.082 ± 0.004	-28.4± 2.9
DPPC150	-	1/150	168.6 ± 7.1	0.124 ± 0.094	-15.7 ± 1.3
PEI/DPPC10	0.016	1/10	166.5 ± 13.9	0.128 ± 0.093	-26.1 ± 0.5
PEI/DPPC20	0.016	1/20	165.4 ± 9.1	0.102 ± 0.006	-31.7 ± 1.2
PEI/DPPC50	0.016	1/50	162.3 ± 13.9	0.124 ±0.041	-28.0 ± 0.7
PEI/DPPC100	0.016	1/100	150.9 ± 30.4	0.106 ± 0.027	-28.0 ± 0.3
PEI/DPPC150	0.016	1/150	146.4 ± 0.3	0.123 ± 0.027	-22.2 ± 2.7

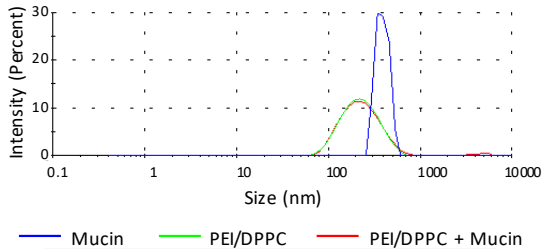

Fig. 1. *In vitro* assessment of mucin interactions with optimized empty DPPC and PEI/DPPC hNPs. **A)** Turbidimetric evaluation (ABS at 650 nm) of the interaction between hNPs with mucin over time. The absorbance at 650 nm of NP dispersions either in water or in a saturated mucin solution are reported as a function of time. **B-C)** Size distribution by intensity of hNP dispersions in water or in saturated mucin solution evaluated by DLS. The size distribution profile of mucin in water is reported as control (**B:** DPPC hNPs and **C:** PEI/DPPC).

Independently of the amount of DPPC added to the organic phase and the presence of PEI in the internal water phase, the adopted formulation conditions lead to the formation of hNPs with a hydrodynamic diameter (D_H) ranging between 135 and 170 nm, monodisperse particle population (PI lower than 0.130) and negative ζ potentials (between -22 and -30 mV). Nevertheless, in each case a flocculation of the exceeding amount of the lipid component was apparent after rotary evaporation of the diffusion solvent under vacuum. This phenomenon was particularly evident when high amounts of DPPC were added to the formulation (i.e., DPPC/PLGA 1/10 w/w), but it was limited up to a theoretical DPPC/PLGA ratio of 1/20. Thus, this ratio was selected for further studies to maximize the amount of DPPC inside the NPs while limiting flocculation. The corresponding formulations, from here on, are named DPPC and PEI/DPPC.

Mucoadhesion studies were performed by measuring the turbidity at 650 nm (ABS) of DPPC and PEI/DPPC hNPs in mucin over time (Fig. 1A). While the ABS of the reference mucin dispersion did not significantly deviate from zero (being within the range 0.040–0.045 arbitrary units), higher values of ABS were observed at each time-point upon addition of hNP dispersions. Nevertheless, no significant differences were observed between ABS of hNPs dispersed in water or in mucin (Fig. 1A). The interactions between mucin and either DPPC or PEI/DPPC hNPS were analysed also by DLS (Fig. 1B and 1C, respectively). The combined particle size distribution for the various replicates shows no change in the position and intensity of the peak.

Characterization of siRNA-loaded PLGA/DPPC hNPs

DPPC and PEI/DPPC formulations were chosen for the encapsulation of siRNA against ENaC at the theoretical loading of 1 nmol/100 mg of hNPs. The addition of siRNA inside the formulation did not result in significant changes of hNP size and PI (Table 2) as compared to empty hNPs (Table 1). siRNA-loaded hNPs with a D_H around 140 nm (141 nm and 142 nm for siRNA-DPPC and siRNA-PEI/DPPC respectively) and low PI were produced with good yields (52 % and 53 % for siRNA-DPPC and siRNA-PEI/DPPC respectively). siRNA was effectively incorporated inside PLGA/DPPC hNPs with a mean entrapment efficiency of 75%. The addition of PEI inside the formulation allowed to reach an excellent entrapment efficiency of 96%, thus increasing siRNA actual loading from 1.35 nmol *per* mg of DPPC hNPs to 1.74 nmol *per* mg of PEI/DPPC hNPs.

Results of *in vitro* release studies performed at physiological pH and temperature (pH 7.2 and 37 °C) are reported in Fig. 2 as percentage of siRNA released over time.

Table 2. Properties of siRNA-loaded PLGA/DPPC hNPs.

	siRNA-DPPC	siRNA-PEI/DPPC
D_H (nm ± SD)	141 ± 0.50	142 ± 1.8
PI (mean ± SD)	0.120 ± 0.018	0.114 ± 0.0050
ζ Potential (mV ± SD)	-29.1 ± 1.6	-29.9 ± 1.4
Yield of production (% ± SD)	52.0 ± 8.9	53.4 ± 2.5
siRNA actual loading [a] (% ± SD)	1.35 ± 0.02	1.74 ± 0.04
Entrapment efficiency (% ± SD)	74.8 ± 1.5	95.9 ± 2.2

[a] siRNA loading was expressed as nmol of encapsulated siRNA *per* 100 mg of hNPs. siRNA theoretical loading was 1 nmol/100 mg of hNPs.

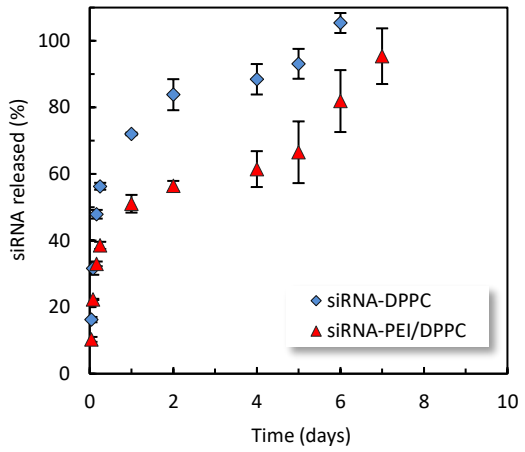

Fig. 2. *In vitro* release kinetics of siRNA from siRNA/DPPC and siRNA-PEI/DPPC in PBS at pH 7.2. Data are expressed as siRNA released (%) ± SD (n=3).

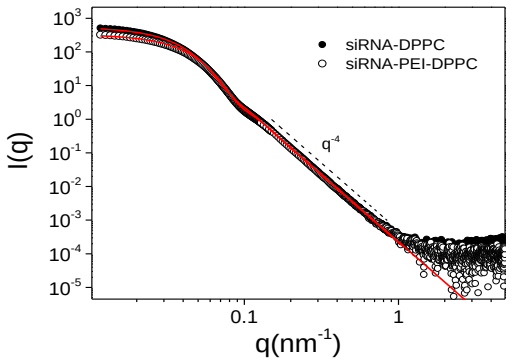

Fig. 3. SAXS specra of siRNA-DPPC (full dots) and siRNA-PEI/DPPC in water (empty dots). The red line is the representative fitting of the siRNA-PEI/DPPC data with the form factor of a polydisperse sphere (red line).

Both siRNA/DPPC and siRNA-PEI/DPPC hNPs displayed a typical triphasic release profile, characterized by an initial burst, with more than 50% of siRNA released in the first hours, followed by a slow release phase lasting a couple of days and a final fast release time period after 4-5 days. Although, both formulations show similar release profile, siRNA/DPPC hNPs provided a significantly more rapid release as compared to siRNA-PEI/DPPC hNPs. Nevertheless, both hNP formulations sustained siRNA release for 1 week.

The I(q) SAXS spectra of siRNA/DPPC and siRNA-PEI/DPPC hNPs are reported in Fig. 3. A low q region affected by the finite size of the particle in the range of the 100 nm distances can be identified. At higher q, an extended region with q^{-4} slope shows up, that identifies a sharp solvent-particle interface and a smooth particles surface. Giunier analysis[25] in the interval 0.0116 $nm^{-1} < q <$ 0.0246nm^{-1} gives gyration radii Rg = 53± 0.5 nm and Rg = 52 ± 0.6 nm for siRNA/DPPC and siRNA/PEI DPPC, respectively. If modeled as spheres, this corresponds to particle radii of 68 nm and 67 nm, in good agreement with hydrodynamic radii (table 2). The best fit of I(q) is obtained by applying the form factor of a distribution of polydisperse spheres with a number-averaged mean radius of 45 ± 9 nm for siRNA/DPPC and of 42 ± 11 nm for siRNA-PEI/DPPC hNPs.

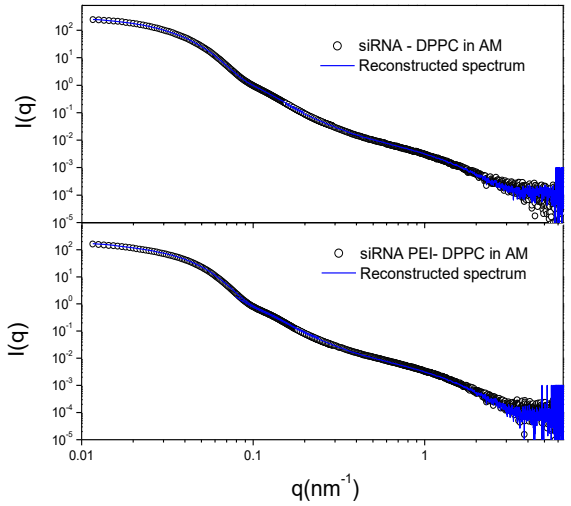

Fig. 4. SAXS spectra of the mixture of siRNA-DPPC (top) and siRNA-PEI/DPPC (bottom) after 12 h of incubation with artificial mucus (AM) (empty dots) *versus* a reconstructed spectrum obtained by summing up AM and naked hNPs spectra (blu line).

The fits are shown in Fig. 3 (red lines). The phospholipid component is possibly coating the PLGA particle, without forming a bilayer envelope. A comparison of the spectra of bare PLGA and PLGA/DPPC particles is reported in *ESI* (Fig. S1) to better illustrate this point. We underline that PEI and siRNA contents are actually of the order of μg over 10 mg of particles, so that scattering contribution from those components are not detectable.

Applying SAXS analysis, the stability of hNPs in mucus was studied during 12 hours after mixing of AM and aqueous dispersions of hNPs in a 3:1 volume ratio. The scattering spectra obtained after equilibration over 12 hours are reported in Fig. 4. Of note, the obtained spectrum is consistent with the sum of the naked particle spectrum and the mucus spectrum that give the reconstructed line shown in the figure (blue line).

In vitro aerosol performance of the optimized hNP formulations was first assessed through NGI on fluorescent $DPPC_{Rhod}$ and $PEI/DPPC_{Rhod}$ hNPs, prepared as described above using PLGA-Rhod (Fig. 5).

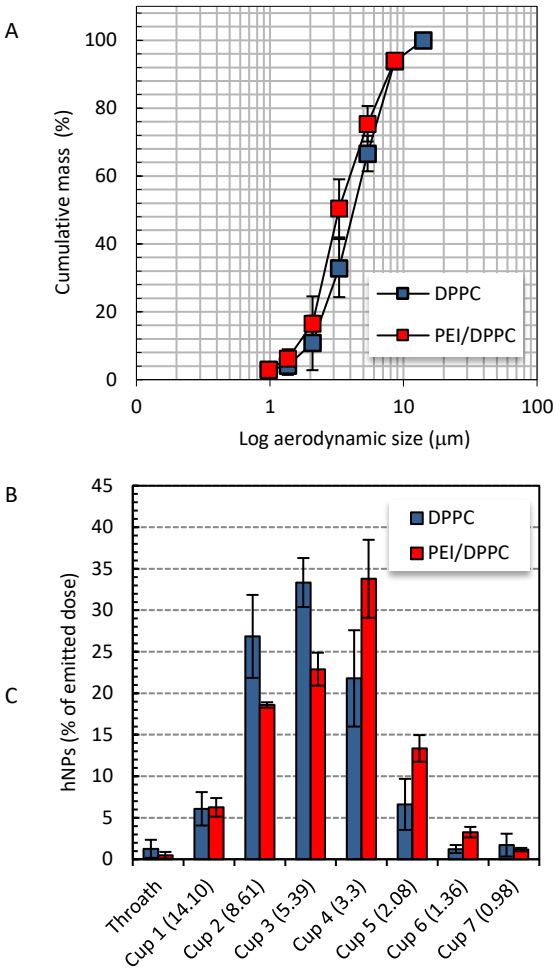

	DPPC	PEI/DPPC
$MMAD_{exp}$ (μm ± SD)	3.96 ± 0.34	3.52 ± 0.20
GSD (± SD)	2.25 ± 0.05	2.26 ± 0.09
FPF (% ± SD)	17.5 ± 2.0	21.5 ± 3.3
RF (% ± SD)	66.4 ± 3.7	73.2 ± 6.9

Fig. 5. *In vitro* aerosol performance of DPPC and PEI/DPPC hNPs upon delivery through the Aeroneb® Go nebulizer. **A)** Cumulative mass recovered as a function of the cut-off diameter of the NGI stages; **B)** NGI deposition pattern; **C)** Fine particle characteristics of the aerosol cloud. Data are presented as mean ± SD (n=3).

Of note, the addition to the formulation of 10 % w/w PLGA-Rhod with respect to the total PLGA amount did not affected hNP properties as compared to non-fluorescent hNPs (data not shown). According to the new regulatory guidance, both USP and Ph.Eur. recognize the suitability of the NGI for nebulizer characterization when used at 15 L/min excluding the pre-separator and placing an internal filter below the MOC.[23]

In this configuration, the seven NGI stages produce cut-off diameters in the range 14.1-0.98 μm, while the last five stages have cut-off diameters between 5.39 and 0.98 μm. Fig. 5A describes the cumulative droplet size distribution of the dose emitted of DPPC and PEI/DPPC hNPs after aerosolization from an Aeroneb® Go vibrating-mesh nebulizer. In both cases, the best fit line was from logarithmic linear regression ($r^2 > 0.96$).

In vitro aerosolization of hNPs on TCCC

Efficiency of aerosolized hNPs to penetrate airway epithelial barrier were probed *in vitro* on the triple cell co-culture. The experiments

B

were carried out on fresh dispersions of freeze-dried hNPs (1:25 hNP/mannitol ratio) in 0.5 mM NaCl for ideal nebulization. To avoid common hNP aggregation in a collapsed cake,[26] mannitol was added to the hNPs as cryoprotectant, and has been chosen amongst others because it induced the lowest variation of D_H and PI with respect to the control, while no difference was observed changing the hNP/cryoprotectant ratio (Table S1 and Fig. S2 in *ESI*). At least in principle, mannitol could work also synergistically with DPPC to facilitate hNP transport through mucus, and in so doing siRNA diffusion, due to its established ability to fluidify mucus.[27]

The stability of hNPs during the nebulisation process was confirmed by TEM analysis of freeze-dried hNPs in the presence of mannitol (1:25 NP/mannitol ratio) before and after nebulization in the Vitrocell® Cloud (Fig. 6).

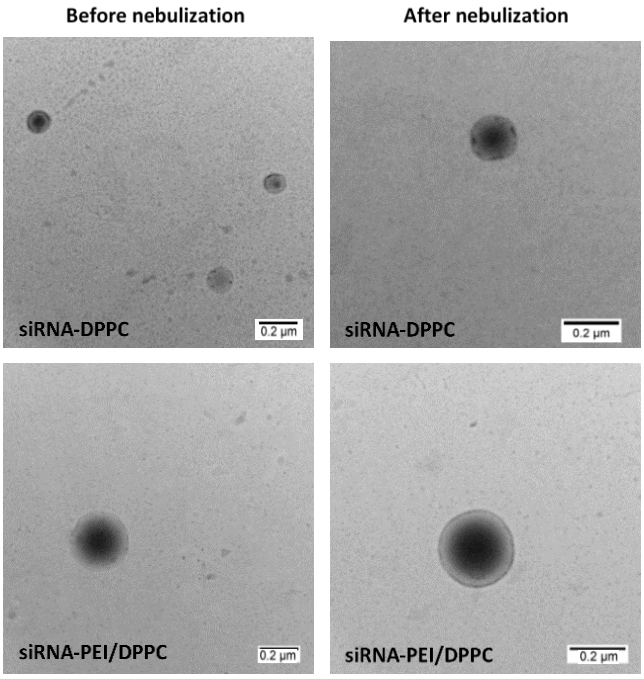

Fig. 6. TEM images of reconstituted freeze-dried siRNA-loaded hNPs (siRNA-DPPC and siRNA-PEI/DPPC) before and after nebulization. Bar is 0.2 µm. Field is representative of the sample.

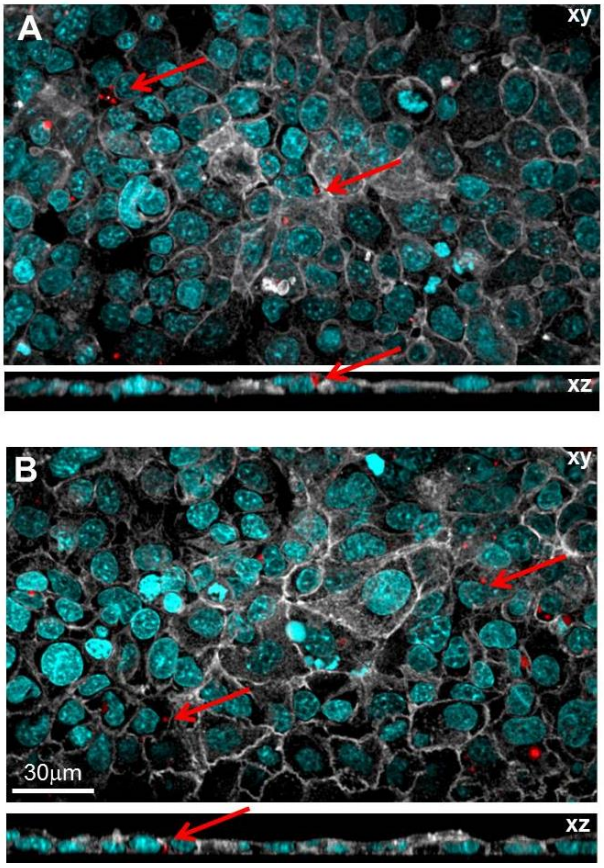

Fig. 7. CLSM images of TCCC after 24h post exposure to 0.5 mg of fluorescently-labelled $DPPC_{Rhod}$ (A) and $PEI/DPPC_{Rhod}$ (B) hNPs deposited after aerosolization. The arrows show hNPs engulfed by the cells.

From TEM images it is apparent that hNPs display a typical core-shell structure characterized by a hydrophobic PLGA core and a DPPC shell. The core-shell structure of the hNPs was retained after the nebulization process, that did not cause any apparent modification of the hNP structure nor hNP aggregation at none of the tested concentrations.

The deposition efficiency was also evaluated for both tested formulations, highlighting in each case a homogeneous distribution of the hNPs on the coverslips inside the exposure chamber (Fig. S3 in ESI) and a direct correlation between the delivered and recovered doses of hNPs. In particular, 0.0051 ± 0.0018 and 0.0127 ± 0.0058 µg/cm² of hNPs were recovered from coverslips after nebulization of low and high concentrations of $DPPC_{Rhod}$, respectively. Meanwhile, likely as a consequence of the good aerosolization properties of $PEI/DPPC_{Rhod}$, 0.0137 ± 0.0092 and 0.0334 ± 0.0069 µg/cm² of hNPs were recovered from coverslips after nebulization of low and high concentrations of PEI-engineered hNPs, respectively.

Uptake of aerosolized hNPs in TCCC

In order to study the cell uptake of the hNPs, fluorescently labelled were erosolized on TCCC. After 24 h post exposure to hNPs, TCCC were visualized by CLSM (Fig. 7). Results indicate that both $DPPC_{Rhod}$ and $PEI/DPPC_{Rhod}$ hNPs (labelled in red) can effectively penetrate into cells and are localized intracellularly (labelled in blue). **TEM?**

Effects of aerosolized hNPs on TCCC

At the tested concentrations, the developed hNPs displayed no significant cytotoxicity as compared to both sodium chloride and mannitol solutions aerosolized at the same concentrations of the samples (*P*>0.5) (Fig. 8 A). On the other hand, a significant cytotoxic effect as compared to TCCC exposed to both low and high hNP concentrations (p<0.001) was observed when the co-cultures were challenged with LPS from *P. aeruginosa* as positive control. These findings were confirmed by CLSM analysis of all treated samples, since no alteration to cell morphology occurred after TCCC exposure to hNPs as compared to the negative control (Fig. S4).

The potential pro-inflammatory effect of aerosolized empty and siRNA-loaded hNPs on TCCC was also investigated by determining TNF-α secretion 24 h post-exposure (Fig. 8B). Of note, exposure to mannitol and empty hNPs, at both low and high concentration, caused a less than 1-fold increase of TNF-α release to the TCCC exposed to 0.5 μM aqueous sodium chloride. As for siRNA-loaded hNPs, we can see at all concentration tested a higher production of TNF-α in comparison to negative control, although values were not significantly different from the mannitol control.

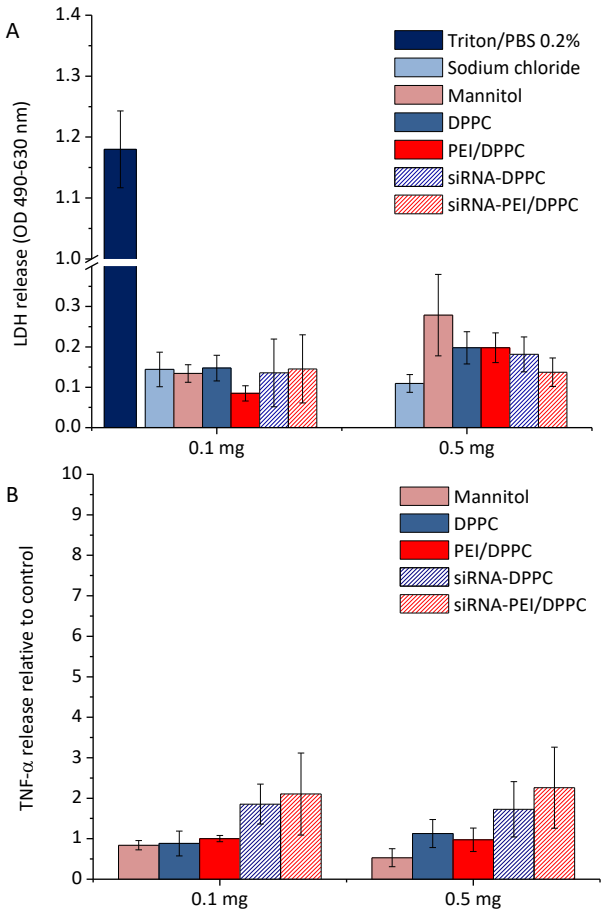

Fig. 8. LDH release (A) and TNF- α secretion (B) of TCCC after 24 h post-exposure to different theoretical amounts (0.1 and 0.5 mg) of aerosolised empty or siRNA-loaded hNPs. Triton 0.2.% (w/v) (A) and LPS 1 μg/mL (B) **DO WE HAVE VALUES?** in PBS were used as positive controls. Sodium chloride was used as negative control. Mannitol aqueous solutions at the same volume and concentrations used for hNP samples were also aerosolized for comparison. LDH data are presented as mean OD values ± S.E.M. of samples diluted 1:10 v/v in cell culture medium (n=3) (**p<0.001). TNF- α data are presented as the mean fold increase of samples relative to the negative control (i.e., sodium chloride) ± S.E.M. (n=3).

Discussion

The importance of lung barriers in determining the therapeutic efficacy of inhaled drugs in severe lung diseases, such as CF, is nowadays acknowledged.[11] A current paradigm suggests that only NPs with appropriate size and surface properties may overcome the complex mucus airway barrier and assist drug interactions with human airway epithelial cells.[28,29] This aspect is particularly crucial for siRNA-based therapeutics, the clinical application of which is further hindered by the short half-life *in vivo* and the low capability to penetrate cell membranes. To overcome these issues, in this work we have designed and developed novel PLGA/DPPC hNPs, containing or not PEI as third component, suitable for pulmonary delivery of siRNA.

The developed PLGA/DPPC hNPs showed a typical core-shell structure,[12] which suggest the presence of a PLGA core surrounded by a lipid shell made of DPPC, independent of the presence of PEI. As demonstrated by hNP/mucus interaction studies, this structure results in non-mucoadhesive or "muco-inert" hNPs, likely able to easily penetrate across the airway mucus layer.[20,21,] Furthermore, the adopted formulation conditions allowed the production of hNPs with a hydrodynamic diameter of 150 nm, which are expected to easily diffuse through the gel-like structure of the mucus.[28,30] Finally, aqueous hNPs were transformed into a solid long-term stable lyophilised powder, which could be re-dispersed in saline without affecting the peculiar NP properties and likely allowing co-administration of a mucus rehydrating agent, such as mannitol.[27]

If DPPC, that is the principal component of the lung lining fluids, is expected to tune hNP interactions with the lung environment, the addition of PEI can play a crucial role for siRNA entrapment inside PLGA/DPPC hNPs. This hypothesis was confirmed by encapsulation studies performed on two siRNA sequences, for α and β ENaC subunits, which have been shown to produce a long term reduction of trans-epithelial Na+ currents and of fluid absorption.[15] In particular, the combination of the two siRNA can expand the lung fluid volume *in vitro*.[16] Of note, siRNA was entrapped inside selected hNPs with high efficiency, particularly when PEI was co-encapsulated. This effect could be likely ascribed to the formation of a complex between PEI, employed at the theoretical N/P ratio of 10, and siRNA.

Information about the presence of PEI/siRNA complexes inside hNPs could not be derived from SAXS spectra, due to the very low amounts of both components. Nevertheless, SAXS analysis clearly demonstrated that the role of PEI in the formulation is not to affect the overall particle morphology, except for a very slight decrease of the average size. On the other hand, the phospholipid component is possibly coating the PLGA particles, as suggested by TEM analysis.

Of note, independently on the presence of PEI inside the formulation, hNPs were stable inside artificial CF mucus at least for 12 hours, confirming, along with in vitro aerosol performance studies, the potential of the system for direct aerosolization on the mucus-lined human airway epithelial barrier.

In fact, to attain maximum siRNA availability at lung epithelial cells, where its target is located, the hNPs should: i) uniformly deposit on the airway epithelium in their stable form; ii) penetrate inside the lung epithelial barrier; iii) interact with the lung epithelium, without compromising cell availability. To draw key information on all these points and to establish *a priori* target formulation parameters for siRNA delivery to human airway epithelium, the behaviour of the developed PLGA/DPPC hNPs after deposition on triple cell co-cultures, which realistically mimic human airway epithelium environment, was investigated.

When human bronchial epithelial cells are grown on porous supports at ALI they reproduce both the *in vivo* morphology and key

physiologic processes, sometimes including tight junctions, basal and mucus cells.[24,31] Furthermore, direct deposition of the aerosolized drug to the apical compartment of the cell culture can be envisaged through systems especially designed for dose-controlled and spatially uniform deposition of liquid aerosols on cells,[32,33] such as the Vitrocell® Cloud here employed. Results showed that the adopted formulation conditions allowed to tune hNP properties, so as to be uniformly and efficiently aerosolized on lung epithelial cells in their integer form. Once landed on the airway barrier, hNPs were demonstrated able to penetrate inside extracellular lung lining fluids, to be taken up by lung epithelial cells without exerting neither a cytotoxic effect or a pro-inflammatory response on the treated lung epithelium model.

Conclusions

In this work, we have successfully designed and developed novel hNPs comprising a PLGA core, likely surrounded by a DPPC shell, with size and surface properties optimized for siRNA transport and delivery at lung. Optimised formulations allowed entrapment of a combination of siRNA against α and β subunits of the ENaC sodium transepithelial channel with high efficiency, which could be optimized by the addition of PEI inside the formulation. The developed hNPs were muco-inert and long-term stable inside mucus. Stable hNP-based dry powders were produced by freeze-drying with mannitol, an osmotic agent of interest for CF treatment. The fate and the effects of hNPs upon *in vitro* deposition on a triple cell co-culture model of the human airway epithelium was thoroughly investigated. Cell uptake studies confirmed the ability of fluorescently labelled hNPs to be internalized inside the airway epithelial barrier. Finally, hNP hazard assessment demonstrated that the developed system does not exert neither cytotoxic nor acute pro-inflammatory effect towards none of the cell components of the co-culture model. Overall, results demonstrate the great potential of PLGA/DPPC hNPs as carriers for siRNA delivery on the human epithelial airway barrier, prompting towards investigation of its therapeutic effectiveness in severe lung diseases.

Acknowledgements

F.U. gratefully acknowledges *Compagnia di San Paolo* and *Istituto Banco di Napoli - Fondazione* (STAR Program, Junior Principal Investigator Grant 2013, Napoli_call2013_35) for financial support. G.C. wishes to thank the International Society for Aerosols in Medicine (ISAM) for the 2015 ISAM Student Fellowships. E.D and B.R.R acknowledge the financial support of the Adolphe Merkle Foundation.

Notes and references

1. J. C. Burnett, J. J. Rossi and K. Tiemann, *Biotechnol. J.,* 2011**, 6**, 1130-1146.
2. S. H. Lee, Y. Y. Kang, H. E. Jang and H. Mok, *Adv. Drug Deliv. Rev.,* 2015.
3. J. G. Karras, G. Sun, J. Tay and A. L. Jackson, *Inflamm. Allergy Drug Targets,* 2013**, 12**, 88-98.
4. J. K. Lam, W. Liang and H. K. Chan, *Adv. Drug Deliv. Rev.,* 2012**, 64**, 1-15.
5. O. M. Merkel, I. Rubinstein and T. Kissel, *Adv. Drug Deliv. Rev.,* 2014**, 75**, 112-128.
6. Y. Singh, S. Tomar, S. Khan, J. G. Meher, V. K. Pawar, K. Raval, K. Sharma, P. K. Singh, M. Chaurasia, R. B. Surendar and M. K. Chourasia, *J. Control Release,* 2015**, 220**, 368-387.
7. D. Cipolla, B. Shekunov, J. Blanchard and A. Hickey, *Adv. Drug Deliv. Rev.,* 2014**, 75**, 53-80.
8. K. Hadinoto, W. S. Cheow, *Colloids Surf. B Biointerfaces.,* 2014**, 116**, 772-785.
9. M. Beck-Broichsitter, O. M. Merkel and T. Kissel , *J. Control Release,* 2012**, 161**, 214-224.
10. F. Ungaro, I. d'Angelo, A. Miro, M. I. La Rotonda and F. Quaglia, *J. Pharm. Pharmacol.,* 2012**, 64**, 1217-1235.
11. I. d'Angelo, C. Conte, M. I. La Rotonda, A. Miro, F. Quaglia and F. Ungaro, *Adv. Drug Deliv. Rev.,* 2014**, 75**, 92-111.
12. K. Raemdonck, K. Braeckmans, J. Demeester and S. C. De Smedt, *Chem. Soc. Rev.,* 2014**, 43**, 444-472.
13. D. Pandita, S. Kumar and V. Lather, *Drug Discov. Today,* 2015**, 20**, 95-104.
14. M. Gunther, J. Lipka, A. Malek, D. Gutsch, W. Kreyling and A. Aigner, *Eur. J. Pharm. Biopharm.,* 2011**, 77**, 438-449.
15. E. Caci, R. Melani, N. Pedemonte, G. Yueksekdag, R. Ravazzolo, J. Rosenecker, L. J. Galietta and O. Zegarra-Moran, *Am. J. Respir. Cell Mol. Biol.,* 2009**, 40**, 211-216.
16. A. Gianotti, R. Melani, E. Caci, E. Sondo, R. Ravazzolo, L. J. Galietta and O. Zegarra-Moran , *Am. J. Respir. Cell Mol. Biol.,* 2013**, 49**, 445-452.
17. F. Blank, B. Rothen-Rutishauser and P. Gehr , *Am. J. Respir. Cell Mol. Biol.,* 2007**, 36**, 669-677.
18. S. Maiolino, F. Moret, C. Conte, A. Fraix, P. Tirino, F. Ungaro, S. Sortino, E. Reddi and F. Quaglia, *Nanoscale,* 2015**, 7**, 5643-5653.
19. T. Narayanan, O. Diat and P. Bosecke, *Nuclear Instruments and Methods in Physics Research Section A: Accelerators, Spectrometers, Detectors and Associated Equipment,* 2001**, 467**, 1005-1009.
20. F. Ungaro, I. d'Angelo, C. Coletta, R. d'Emmanuele di Villa Bianca, R. Sorrentino, B. Perfetto, M. A. Tufano, A. Miro, M. I. La Rotonda and F. Quaglia, *J. Control Release,* 2012**, 157**, 149-159.
21. I. d'Angelo, B. Casciaro, A. Miro, F. Quaglia, M. L. Mangoni and F. Ungaro, *Colloids Surf. B Biointerfaces,* 2015**, 135**, 717-725.
22. P. C. Griffiths, B. Cattoz, M. S. Ibrahim and J. C. Anuonye, *Eur. J. Pharm. Biopharm.,* 2015**, 97**, 218-222.
23. V. A. Marple, B. A. Olson, K. Santhanakrishnan, D. L. Roberts, J. P. Mitchell and B. L. Hudson-Curtis, *J. Aerosol Med.,* 2004**, 17**, 335-343.
24. A. D. Lehmann, N. Daum, M. Bur, C. M. Lehr, P. Gehr and B. M. Rothen-Rutishauser, *Eur. J. Pharm. Biopharm.,* 2011**, 77**, 398-406.

25. G. Guinier, G. Fournet , *Small angle scattering of X rays,* John Wiley & sons, New York,1955.
26. P. Fonte, S. Reis and B. Sarmento, *J. Control Release,* 2016**, 225**, 75-86.
27. S. J. Nolan, J. Thornton, C. S. Murray and T. Dwyer, *Cochrane. Database. Syst. Rev.,* 2015**, 10**, CD008649.
28. L. M. Ensign, B. C. Tang, Y. Y. Wang, T. A. Tse, T. Hoen, R. Cone and J. Hanes, *Sci. Transl. Med.,* 2012**, 4**, 138ra79.
29. I. d'Angelo, C. Conte, A. Miro, F. Quaglia and F. Ungaro, *Curr. Top. Med. Chem.,* 2015**, 15**, 386-400.
30. S. K. Lai, Y. Y. Wang, K. Hida, R. Cone and J. Hanes, *Proc. Natl. Acad. Sci. U. S. A,* 2010**, 107**, 598-603.
31. B. M. Rothen-Rutishauser, S. G. Kiama and P. Gehr, *Am. J. Respir. Cell Mol. Biol.,* 2005**, 32**, 281-289.
32. C. Endes, O. Schmid, C. Kinnear, S. Mueller, S. Camarero-Espinosa, D. Vanhecke, E. J. Foster, A. Petri-Fink, B. Rothen-Rutishauser, C. Weder and M. J. Clift, *Part Fibre. Toxicol.,* 2014**, 11**, 40.
33. C. Endes, S. Mueller, C. Kinnear, D. Vanhecke, E. J. Foster, A. Petri-Fink, C. Weder, M. J. Clift and B. Rothen-Rutishauser, *Biomacromolecules.,* 2015**, 16**, 1267-1275.